



# Active galactic nuclei imaging programs of the *RadioAstron* mission

Gabriele Bruni<sup>a,\*</sup>, Tuomas Savolainen<sup>b,c,d</sup>, Jose Luis Gómez<sup>e</sup>, Andrei P. Lobanov<sup>d</sup>  
Yuri Y. Kovalev<sup>f,g,d</sup>, On behalf of the RadioAstron AGN imaging KSP teams

<sup>a</sup> INAF – Istituto di Astrofisica e Planetologia Spaziali, via del Fosso del Cavaliere 100, 00133 Rome, Italy

<sup>b</sup> Aalto University Department of Electronics and Nanoengineering, PL 15500, FI-00076 Aalto, Finland

<sup>c</sup> Aalto University Metsähovi Radio Observatory, Metsähovintie 114, 02540 Kylmälä, Finland

<sup>d</sup> Max-Planck-Institut für Radioastronomie, Auf dem Hügel 69, 53121 Bonn, Germany

<sup>e</sup> Instituto de Astrofísica de Andalucía, CSIC, Glorieta de la Astronomía s/n, 18008 Granada, Spain

<sup>f</sup> Astro Space Center of Lebedev Physical Institute, Profsoyuznaya St. 84/32, 117997 Moscow, Russia

<sup>g</sup> Institute of Physics and Technology, Dolgoprudny, Institutsky per., 9, Moscow region, 141700, Russia

Received 24 December 2018; received in revised form 28 March 2019; accepted 30 March 2019

Available online 11 April 2019

## Abstract

Imaging relativistic jets in active galactic nuclei (AGN) at angular resolution significantly surpassing that of the ground-based VLBI at centimetre wavelengths is one of the key science objectives of the *RadioAstron* space-VLBI mission. There are three *RadioAstron* imaging key science programs that target both nearby radio galaxies and blazars, with one of the programs specifically focusing on polarimetry of the jets. The first images from these programs reach angular resolution of a few tens of microarcseconds and reveal unprecedented details about the jet collimation profile, magnetic field configuration, and Kelvin-Helmholtz instabilities along the flow in some of the most studied AGN (3C84, BL Lac, 3C273, S50836 + 710). Here we give an overview of the goals and strategy of these three ongoing programs, highlight their early results, and discuss the challenges of space-VLBI imaging.

© 2019 COSPAR. Published by Elsevier Ltd. All rights reserved.

**Keywords:** Techniques; Radio interferometry; Active galactic nuclei

## 1. Introduction

Launched in 2011, *RadioAstron* is a mission to realize a very long baseline interferometry (VLBI) array that combines ground radio telescopes with a 10-m Space Radio Telescope (SRT) on a highly elliptical orbit around the Earth (Kardashev et al., 2013). The antenna is equipped with four different on-board receivers, operating at 1.19–1.63 cm (K-band), 6.2 cm (C-band), 18 cm (L-band), and 92 cm (P-band). The apogee height of the orbit of Spektr-R

spacecraft carrying the SRT is up to 360,000 km, which means that minimum spacing of interferometric fringes on the sky can be as small as 7  $\mu$ as at the *RadioAstron*'s highest observing frequency of 22 GHz. This makes *RadioAstron* the highest angular resolution instrument in the history of astronomy and allows one to probe a previously unexplored parameter space for black hole powered jets in active galactic nuclei, pulsars, and galactic as well as extragalactic masers (Kardashev et al., 2017).

At the beginning of *RadioAstron* open science program in 2013, three key science programs (KSP; essentially large projects with legacy value) carrying out space-VLBI imaging of AGN were conceived to exploit the ultra-high angular resolution and polarimetry capabilities of the mission. The key scientific drivers of these programs were:

\* Corresponding author.

E-mail addresses: [gabriele.bruni@inaf.it](mailto:gabriele.bruni@inaf.it) (G. Bruni), [tuomas.k.savolainen@aalto.fi](mailto:tuomas.k.savolainen@aalto.fi) (T. Savolainen), [jlgomez@iaa.es](mailto:jlgomez@iaa.es) (J.L. Gómez), [alobanov@mpifr-bonn.mpg.de](mailto:alobanov@mpifr-bonn.mpg.de) (A.P. Lobanov), [yyk@asc.rssi.ru](mailto:yyk@asc.rssi.ru) (Y.Y. Kovalev).

- Resolving the jets in a few nearby AGN down to spatial scales of a few to a few hundred gravitational radii ( $r_g$ ) from the black hole (Nearby AGN KSP; PI: T. Savolainen). Measuring the size, shape and internal structure of the region where the jet is accelerated and collimated provides a way to test the current models for jet formation in accreting black holes and answer questions like “do the current general relativistic magnetohydrodynamic simulations of jet formation (e.g., Tchekhovskoy et al., 2011) capture all the relevant physics of the system” and “are the jets powered by accretion (Blandford and Payne, 1982) or by rotational energy of the black hole itself (Blandford and Znajek, 1977)”.
- Transversely resolving the internal jet structure in powerful blazars and tracing shocks and plasma instabilities developing in the flow (Powerful AGN KSP; Co-PIs: A. P. Lobanov and M. Perucho). Measuring the detailed morphology of the instability patterns and their comparison to earlier space-VLBI observations by the Japanese VSOP program (e.g., Lobanov and Zensus, 2001) can help to distinguish between different plasma instabilities and consequently to constrain the physical conditions of the jet and the ambient medium.
- Using ultra-high angular resolution multi-frequency polarization imaging to probe the jet magnetic field structure in or close to the jet acceleration and collimation zone (AGN polarization KSP; PI: J.L. Gómez). In the current view of jet formation, the jets are highly magnetized with an ordered large-scale field near the launching site (Tchekhovskoy et al., 2011; Zamaninasab et al., 2014), but the evolution of the magnetization and magnetic field structure further downstream is much less clear. Being able to transversely resolve the jets at multiple frequencies allows one to con-

strain the magnetic field structure by analyzing spatially resolved linear polarization spectra (e.g., Zamaninasab et al., 2013; Gómez et al., 2016).

In this paper we give an overview of these three programs, their early results, and of the technical challenges of imaging observations with a space-VLBI satellite on a high orbit.

## 2. Observations

The three imaging programs have been running since 2013 and observations have been approved until 2019. The largest number of observed sources (ten; see Table 1) are in the polarization program, while the number of targets in the two other programs is more modest. Three nearby AGN were observed at multiple frequencies and epochs: 1.6 GHz (M87 in 2014), 4.8 GHz (M87 in 2014, 3C84 in 2013, Cen A in 2014) and 22 GHz (M87 in 2014 and 2018, 3C84 in 2013 and 2016, Cen A in 2014). Furthermore, three powerful blazars (0836 + 710, 3C273, 3C345) were observed in 2013–2014 using the (non-polarimetric) dual-band mode of *RadioAstron*.

All the imaging observations were carried out when the SRT was close to its perigee. Since the orbital velocity of the satellite is the highest near the perigee, it is possible to cover a wide range of ground-to-space baseline lengths, from less than one Earth diameter up to about ten Earth diameters, within a day. This is essential for the *RadioAstron* imaging programs which are generally challenging due to the very sparse sampling of the  $(u, v)$  coverage for the ground-to-space baselines (see Fig. 1). Continuous  $\sim 24$  h long observations around the perigee passage require multiple tracking stations (Puschino near Moscow, Russia and Green Bank in West Virginia, USA; Kardashev

Table 1  
Details on observations performed in the framework of the AGN polarization KSP.

Target	Date	Exp.	Band	Corr.	Status and complementary obs.
0642 + 499	03/2013	GK047	L	Yes	Lobanov et al. (2015)
BL Lac	09/2013	GA030A	L	Yes	Data analysis
BL Lac	11/2013	GA030B	K	Yes	Gómez et al. (2016)
3C273	01/2014	GA030C	K	Yes	Bruni et al. (2017)
3C273	06/2014	GA030F	L	Yes	Bruni et al. (in prep.)
3C279	03/2014	GA030D	K	Yes	Data analysis
OJ287	04/2014	GA030E	K	Yes	Gómez et al. (in prep.)
0716 + 714	01/2015	GL041A	K	Yes	Kravchenko et al. (in prep.)
3C345	03/2016	GG079A	L	Yes	Data analysis
OJ287	04/2016	GG079B	L	Yes	Data analysis
OJ287	04/2016	GG079C	K	No	Processing
3C345	05/2016	GG079D	K	No	Processing
3C454.3	10/2016	GG081A	K	No	Processing, GMVA
CTA102	10/2016	GG081B	K	No	Processing, GMVA
OJ287	03/2017	GG081C	K	Yes	Processing, EHT + ALMA and GMVA + ALMA
BL Lac	10/2017	GG083A	K	No	Processing, GMVA
3C279	01/2018	GG083B	K	No	Processing, GMVA + ALMA
3C120	02/2018	GG083C	K	No	Processing, GMVA
3C273	02/2018	GG083D	K	No	Processing, GMVA + ALMA
OJ287	04/2018	GG083E	K	No	Processing, EHT + ALMA and GMVA + ALMA

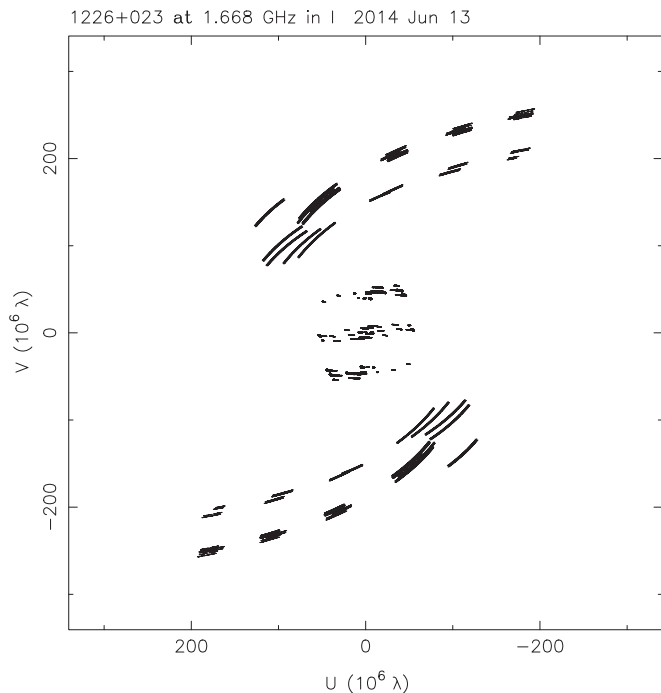


Fig. 1. An example  $(u, v)$  coverage of *RadioAstron* 3C273 observations at L-band, performed within the AGN polarization KSP (ra\_ks04f). The central bulge, given by the ground array, traces about one Earth diameter, while wings are given by the *RadioAstron* baselines. The maximum length of a space baseline in this figure is  $\sim 4.5D_{\text{Earth}}$ .

et al., 2013; Ford et al., 2014) and large ground radio telescopes over a wide range of longitudes in order to guarantee that there is always a common visibility between the SRT and a sensitive ground radio telescope. Sensitive baselines are crucial for finding the typically weak ground-to-space interferometric signal, i.e., fringes.

Due to these requirements, *RadioAstron* imaging observations were typically supported on the ground by a global VLBI array including 15–30 antennas from the major astronomical cm-wavelength VLBI facilities: European VLBI Network (EVN) in Europe, Asia and Africa, Very Long Baseline Array (VLBA) in the United States, Long Baseline Array (LBA) in Australia, Kvazar Array in Russia, and Korean VLBI Network (KVN) in Korea. Furthermore, several large standalone radio observatories participated in the observations: Very Large Array (VLA), Green Bank Telescope and Arecibo in United States, Kalyazin in Russia, Usuda in Japan and Deep Space Network stations in Robledo, Spain and Tidbinbilla, Australia. The typical observing setup of the ground-based antennas was matched to the two 16 MHz wide IFs of the SRT, but instead of the one-bit sampling of the *RadioAstron* data, the ground array data were sampled with two bits. Therefore, in the typical observation *RadioAstron* recorded data at the rate of 128 Mbps, while the ground array recorded at 256 Mbps. However, in polarimetric observations larger bandwidths were often used at the ground array in order to facilitate Faraday rotation measurements.

Since the imaging observations are limited to about 10% of the full orbital period of 8.5 days and since the part of the sky that is visible at any given time is limited by a number of physical and operational constraints, scheduling of *RadioAstron* imaging experiments is challenging. One may have to wait for the orbit to evolve for a year or more in order to find a date that provides sufficiently good  $(u, v)$  coverage for a particular target. This, in addition to the required substantial ground resources, typically limits the number of imaging experiment to a handful per year.

### 3. Data processing

The raw data from the different antennas participating in the imaging experiments were transferred to Max Planck Institute for Radio Astronomy (MPIfR) in Bonn, Germany, for correlation (see Müskens et al., 2016 for details on the correlator hardware and operation). Due to the nature of space-VLBI data, customized correlation and data reduction procedures are necessary, as explained below.

#### 3.1. Correlation of space-VLBI data

A modified version of the DiFX software correlator for VLBI (Deller et al., 2011), able to combine ground and space antennas, was developed at the MPIfR. Among other features, this version can deal with data from an orbiting antenna, properly calculating data transmission delays as well as the general relativistic corrections for the delay model due to the Earth and Moon gravitational fields. Furthermore, a fringe-search window much wider than that provided by previous software can be used at the correlator stage, in order to look for signals with delay and delay-rate more than one order of magnitude larger than usually found for ground baselines. Indeed, uncertainties in the orbit reconstruction can easily lead to large discrepancies with respect to the expected fringe peak position. A complete description of the software is given in Bruni et al. (2016). In case signal is not found at the longest space baselines, a best guess for delay and delay rate is extrapolated from the part of the experiment giving high-SNR fringes (typically when the SRT is close to the perigee), and a wider than usual correlation window (shorter integration time and smaller width of the spectral channels) is applied. This allows for further fringe search with post-processing software.

#### 3.2. Calibration and imaging

Once data are correlated, a standard FITS file is produced that can be imported for calibration with the PIMA<sup>1</sup> (Petrov et al., 2011) or AIPS<sup>2</sup> (Greisen, 2003) interferometric data reduction and analysis packages and subsequently

<sup>1</sup> <http://astrogeo.org/pima/>.

<sup>2</sup> <http://www.aips.nrao.edu/index.shtml>.

for imaging with e.g., the DIFMAP<sup>3</sup> (Shepherd, 1997) software.

One of the crucial steps in calibrating the space-VLBI data is searching for the often weak fringes on the noisy ground-to-space baselines. This requires techniques that are usually not necessary in the standard ground-VLBI fringe fitting. As mentioned before, delay and delay rate may significantly differ from the predicted values (up to  $\sim 2 \mu\text{s}$  and  $7 \times 10^{-11}$  s/s, respectively) due to inaccuracies in the SRT orbit prediction, which requires large fringe search windows. Secondly, the residual phase delay may have a significant second-order time dependence over the 10 min scan lengths mostly this is an issue when the satellite is close to the perigee and its motion vector changes rapidly. This so-called *acceleration* term can lead to decorrelation and in rare cases even to the loss of fringes. For many of the observed blazars the time variable delay rate is not a major problem, since they can often be detected with short enough integration time ( $< 1$  min) so that average decorrelation due to the acceleration term remains small ( $< 1\%$  for accelerations of  $< 1$  mHz/s, see Bruni et al. (2016) for an example of this effect). However, the more resolved jets in the nearby AGN KSP require long integration times (often  $\sim 10$  min) in fringe-fitting of the ground-to-space data. Fortunately, PIMA is able to simultaneously solve for the acceleration term in addition to group delay and rate and it was used in the fringe search of the nearby AGN targets (e.g., 3C84; Giovannini et al., 2018).

The bright target sources of the *RadioAstron* AGN imaging programs can usually be easily detected on the ground-to-ground baselines. Therefore, we could in principle phase up the ground array and search for fringes between this coherently averaged signal and the SRT, which would lead to a reduction in the detection threshold. It turns out that the same reduction can be achieved by global fringe-fitting, if the ground-to-ground baselines are much more sensitive than the ground-to-space baselines (Kogan, 1996). We have taken advantage of this by using an iterative fringe-fitting procedure. The ground-VLBI data are first processed in the standard manner, yielding a phase-calibrated data set and an image, which are used as inputs in the second round of global fringe-fitting. Fringes to the SRT are searched using multiple baseline combinations, so-called baseline stacking, which lowers the detection threshold. Furthermore, since the ground array data are already calibrated – removing much of the short term atmospheric phase fluctuations<sup>4</sup> – it is possible to coherently average the data for the typical scan length of 10 min.<sup>5</sup> This procedure can enhance the sensitivity of

space baselines, yielding fringe detections on baselines as long as 7–8 Earth diameters ( $D_{\text{Earth}}$ ) as in the case of the BLLac observations in the AGN polarization program (Gómez et al., 2016) and 3C84 observations in the nearby AGN program (Giovannini et al., 2018).

There are also a few important aspects of the *RadioAstron* data that need to be taken into account when carrying out imaging and self-calibration steps. First, using natural weighting of the visibility data leads to a very small contribution to the image from the space baselines. This can be offset by weighting by the inverse of the local visibility sampling density in the  $(u, v)$  plane. This so-called *uniform* weighting can be tuned by adjusting the bin size in the  $(u, v)$  plane over which the weights are determined. For space-VLBI, it is often beneficial to increase the bin size compared to what is used in the ground-only imaging. This is known as *super-uniform* weighting and it enhances the contribution of the long ground-to-space baselines.<sup>6</sup> Secondly, if the signal-to-noise ratio on the ground-to-space baselines is low, it is dangerous to carry out phase self-calibration for the SRT using solution intervals as short as typically applied to the ground-array data ( $\sim 10$  s). Using a short phase self-calibration solution interval can lead to a generation of spurious flux from the noise on the ground-to-space baselines, if the baselines to the SRT are much longer than any of the ground-to-ground baselines (for the general discussion of the effect, see Martí-Vidal and Marcaide, 2008). Luckily, the SRT is outside of the atmosphere and hence it suffers much less from the short time scale phase fluctuations than the ground-based telescopes. Hence, we used as long as 2 min phase self-calibration solution interval for the SRT if the ground-to-space data had low SNR. Amplitude self-calibration of the SRT was typically limited to solving a single gain scaling factor for the whole observation.

#### 4. Early results from the AGN imaging KSPs

In the following, we give a brief summary of the work done since 2013 in the framework of the three KSPs, and the main results achieved to date.

##### 4.1. AGN polarization KSP

The AGN polarization KSP has been performing observations since the Early Science Period (ESP). With more than 20 experiments to date, it targeted several AGN with prominent polarimetric properties (see Table 1). During the ESP, the polarimetry capabilities of *RadioAstron* were tested at L-band on 0642 + 499 (Lobanov et al., 2015), finding a stable instrumental polarization within 9%, consistent between the two IFs. During the AO-1 period (July 2013–June 2014), the first 22 GHz polarimetric

<sup>3</sup> <ftp://ftp.astro.caltech.edu/pub/difmap/difmap.html>.

<sup>4</sup> We note that after self-calibration, the ground array data still contain phase fluctuations due to the atmosphere over the *reference antenna*. However, this effect can often be minimized by selecting a well-behaved reference station.

<sup>5</sup> Assuming that the acceleration term is small or already corrected.

<sup>6</sup> Sometimes the term “super-uniform” is also used to refer to *not* scaling the weights by visibility amplitude errors.

observations on BL Lac were performed, giving fringes up to  $\sim 8D_{\text{Earth}}$ , and resulting in the highest angular resolution image to date (21  $\mu\text{s}$ , see Fig. 2, from Gómez et al. (2016)). Again, an instrumental polarization below 9% was found, allowing one to use standard procedures to correct it. The resulting polarimetric image, combined with quasi-simultaneous ground-based polarimetric VLBI imaging at 15 GHz and 43 GHz, showed evidence for a large-scale helical magnetic field threading the jet. Moreover, evidence for emission from a (re-) collimation shock at 40  $\mu\text{s}$  upstream of the core was found. Further observations from the AO-1 period revealed a two orders of magnitude drop in the brightness temperature of 3C273 (Bruni et al., 2017) when compared to *RadioAstron* observations performed with a similar configuration only one year before (Kovalev et al., 2016; Johnson et al., 2016). Furthermore, 1.6 GHz and 4.8 GHz observations on the same target revealed a limb-brightened jet, with a sheath emission dominating at 1.6 GHz, and a spine emission at 4.8 GHz (Bruni et al. in prep.). Observations from the AO-2 period (July 2014 – June 2015) of S50716 + 71 probed the inner 100  $\mu\text{s}$  of the blazar jet, detecting polarized emission up to  $5.6D_{\text{Earth}}$  space baselines, and a core brightness temperature exceeding the theoretical limits (see the contribution from Kravchenko et al.).

Starting from 2017, close-in-time 86 and 230 GHz observations at tens of  $\mu\text{s}$  resolution with the Global mm-VLBI Array and the Event Horizon Telescope (Fish et al., 2016) including the phased ALMA array have been providing unique data sets that will explore the jet structure and polarization properties of several AGN from 22 GHz up to 300 GHz.

#### 4.2. Nearby AGN KSP

Nearby AGN key science program is aimed at obtaining images with a *spatial* resolution of a few to a few hundred gravitational radii in nearby radio galaxies 3C84 ( $D_L = 75$  Mpc), M87 ( $D_L = 16$  Mpc), and Cen A ( $D_L = 4$  Mpc). All targets have been observed at multiple *RadioAstron* bands and at multiple epochs. Ground-to-space fringes have been successfully found for 3C84 at 4.8 and 22 GHz, and for M87 at 1.6, 4.8 and 22 GHz. Two experiments on Cen A at 4.8 and 22 GHz did not yield ground-to-space fringes.

The early dual-band observations of 3C84, the central galaxy of Perseus cluster, in 2013 resulted in fringe detections on ground-to-space baselines as long as  $8D_{\text{Earth}}$  at both 4.8 GHz (Savolainen et al. in prep.) and 22 GHz (Giovannini et al., 2018, see also Fig. 3). With 27  $\mu\text{s}$  fringe spacing, the 22 GHz *RadioAstron* observations transversely

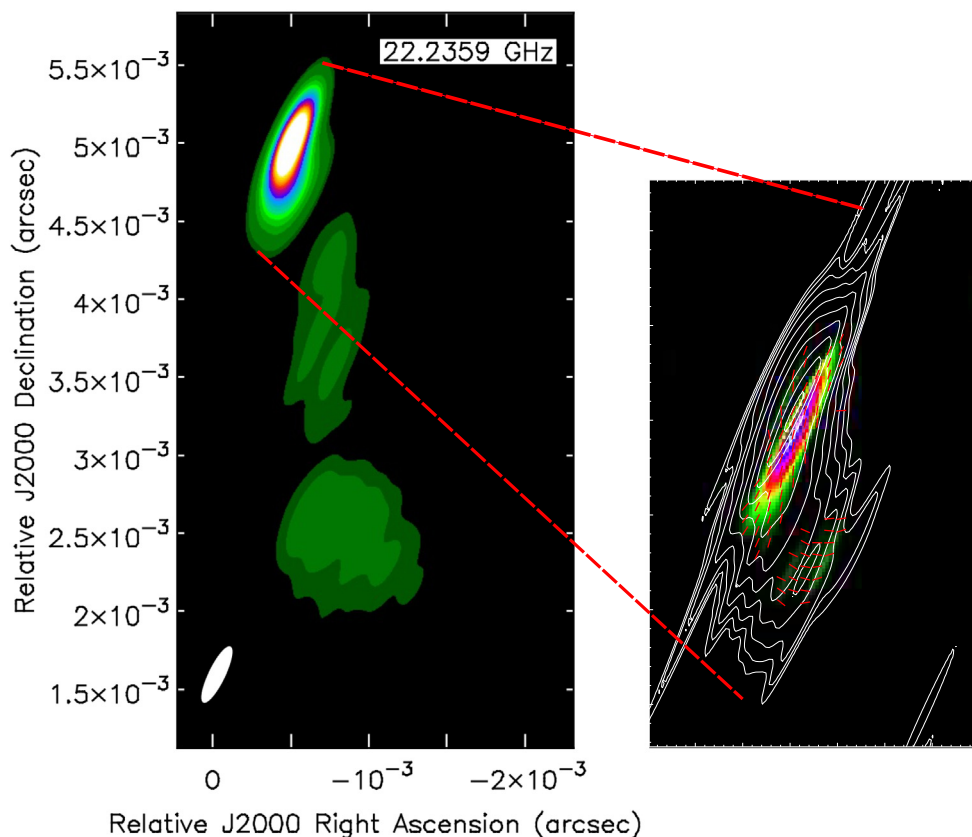


Fig. 2. Images of BL Lac at 22 GHz from the AGN polarization KSP (Gómez et al., 2016). Left panel: natural weighting, resulting in a synthesized beam of  $390 \times 100 \mu\text{s}$ ; right panel: zoom on the core region in super-uniform weighting, reaching a resolution of  $260 \times 21 \mu\text{s}$ , with linearly polarized emission shown in colors, total intensity in contours, and Electric Vector Position Angle (EVPA) as red bars. (For interpretation of the references to colour in this figure legend, the reader is referred to the web version of this article.)

resolved the edge-brightened jet of 3C 84, and allowed measuring the jet collimation profile down to  $\sim 10^2 r_g$  from the central black hole. The reconstructed image revealed an initially very broad jet with a transverse radius  $\gtrsim 250 r_g$  at merely  $350 r_g$  from the core, which implies that the jet is either rapidly laterally expanding on scales below  $\sim 10^2 r_g$  or the outer layer of the jet is launched from the accretion flow and not from the ergosphere of the spinning black hole. The measured collimation profile is almost cylindrical and it clearly differs from the parabolic profiles measured for M87 (Nakamura et al., 2018) and Cyg A (Boccardi et al., 2016). We believe that this is likely due to the re-started nature of the jet in 3C 84: the bright feature ejected from the VLBI core around 2003 could be a parsec scale analogue of a kiloparsec scale hot spot, i.e., the point where the jet rams into the external medium, slows down and dissipates a significant fraction of its energy (Giovannini et al., 2018; Nagai et al., 2017). Kiloparsec scale jets can collimate to an almost cylindrical shape before entering the hot spot due to the uniform pressure cavity that the jet has created around it (Komissarov and Falle, 1998) and we may see the same effect at parsec scale in 3C 84. The 4.8 GHz *RadioAstron* image shows low luminosity, cocoon-like emission around the re-started parsec-scale jets, which supports this explanation (Savolainen et al. in prep.).

In June 2014, there was an opportunity to obtain an exceptionally good  $(u, v)$  coverage in space for the nearby radio galaxy M87. The observations carried out at 1.6 GHz together with 26 ground radio telescopes resulted in ground-to-space fringe detections up to  $5 D_{\text{Earth}}$ . The reconstructed high-dynamic-range images have a beam size of 1–2 mas depending on the applied weights. They allow detailed mapping of the rich internal structure of the 450 mas long jet, which is resolved in transverse direction by 4–12 resolution elements and appears to contain helical threads or filaments (Savolainen et al. in prep.). Data processing and analysis of the other M87 observations, including the 22 GHz polarimetric observation that was carried out in May 2018 – close-in-time to the Event Horizon Telescope observations of M87 at 230 GHz – are still ongoing at the time of writing.

#### 4.3. Powerful AGN KSP

First results from this programme have been submitted at the time of writing, presenting L, C, and K-band observations of S5 0836 + 710 (Vega-García et al. subm.). A detailed study of the Kelvin–Helmholtz instabilities along the jet, on angular scales between 0.02 and 200 mas, was performed, resulting in an indication of helical instability

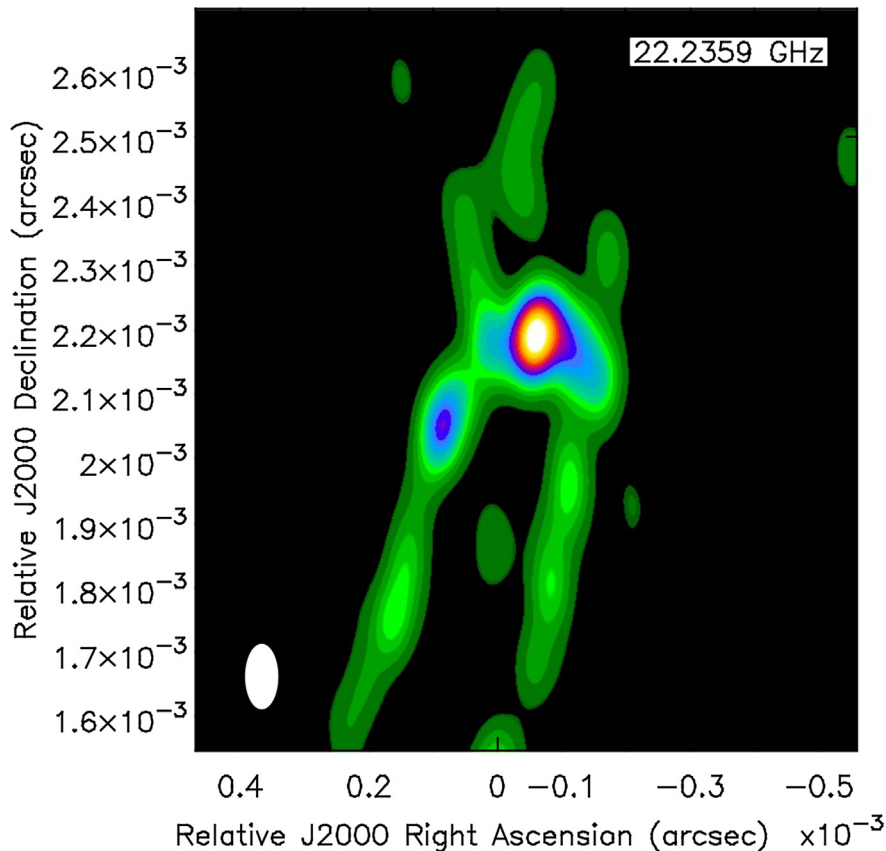


Fig. 3. Image of the nuclear region of 3C84 at 22 GHz, as seen by *RadioAstron* at angular resolution of  $100 \times 50 \mu\text{as}$  (Giovannini et al., 2018). A large transverse jet radius of  $\gtrsim 250 r_g$  at only  $350 r_g$  from the core was measured.

modes. All observations were carried out during AO-1 and AO-2, including also 3C273, 3C345, and 4C + 69.21. See the contribution from Zensus et al. for further details on the results of this KSP.

## 5. Future prospects

Recent inclusion of phased Atacama Large Millimeter/submillimeter Array (ALMA) in global VLBI networks at short mm-wavelengths now offers high sensitivity for tens of  $\mu\text{s}$  resolution imaging from the ground (Matthews et al., 2018). With ALMA, the Global mm-VLBI Array at 86 GHz and the Event Horizon Telescope at 230 GHz give an opportunity to obtain multi-frequency polarization imaging at angular resolution comparable to the *RadioAstron* one. Such data can be used to constrain the magnetic field structure close to the jet base via the analysis of spatially resolved polarization spectra.

In the future, the *Millimetron* space observatory (Kardashev et al., 2014), led by the Astro Space Center of the Lebedev Physical Institute, is planned to perform space-VLBI observations at mm-wavelengths. In the VLBI-mode the angular resolution of *Millimetron* observations is in principle high enough to resolve black hole silhouettes at the centers of AGN up to a distance of  $\sim 100$  Mpc, and probe at unprecedented resolution the matter outflows and magnetic field structure in the vicinity of the events horizon.

## Acknowledgments

GB acknowledges financial support under the INTEGRAL ASI-INAF agreement 2013-025-R.1. TS was supported by the Academy of Finland projects 274477, 284495, and 312496. The RadioAstron project is led by the Astro Space Center of the Lebedev Physical Institute of the Russian Academy of Sciences and the Lavochkin Scientific and Production Association under a contract with the State Space Corporation ROSCOSMOS, in collaboration with partner organizations in Russia and other countries. This research is based on observations processed at the Bonn Correlator, jointly operated by the Max Planck Institute for Radio Astronomy (MPIfR) and the Federal Agency for Cartography and Geodesy (BKG). The National Radio Astronomy Observatory is a facility of the National Science Foundation operated under cooperative agreement by Associated Universities, Inc. The European VLBI Network is a joint facility of independent European, African, Asian, and North American radio astronomy institutes.

## References

Blandford, R.D., Znajek, R.L., 1977. Electromagnetic extraction of energy from Kerr black holes. *MNRAS* 179, 433–456.  
 Blandford, R.D., Payne, D.G., 1982. Hydromagnetic flows from accretion disks and the production of radio jets. *MNRAS* 199, 883–903.

Boccardi, B., Krichbaum, T.P., Bach, U., et al., 2016. The stratified two-sided jet of Cygnus A. Acceleration and collimation. *A&A* 585, 33.  
 Bruni, G., Anderson, J., Alef, W., et al., 2016. The RadioAstron Dedicated DiFX Distribution. *Galaxies* 4, 55.  
 Bruni, G., Gómez, J.L., Casadio, C., et al., 2017. Probing the innermost regions of AGN jets and their magnetic fields with RadioAstron. II. Observations of 3C 273 at minimum activity. *A&A* 604, A111.  
 Deller, A.T., Brisken, W.F., Phillips, C.J., et al., 2011. DiFX-2: a more flexible, efficient, robust, and powerful software correlator. *PASP* 123, 275–287.  
 Fish, V., Akiyama, K., Bouman, K., et al., 2016. Observing—and imaging—active galactic nuclei with the event horizon telescope. *Galaxies* 4, 54.  
 Ford, H.A., Anderson, R., Belousov, K., et al., 2014. The RadioAstron Green Bank Earth Station. Ground-based and Airborne Telescopes V. In: Stepp, Larry M., Gilmozzi, Roberto, Hall, Helen J. (Eds.), *Proc. of SPIE, SPIE, Bellingham, Washington, USA*, vol. 9145, 91450B.  
 Giovannini, G., Savolainen, T., Orienti, M., et al., 2018. A wide and collimated radio jet in 3C84 on the scale of a few hundred gravitational radii. *Nat. Astron.* 2, 472–477.  
 Gómez, J.L., Lobanov, A.P., Bruni, G., et al., 2016. Probing the innermost regions of AGN jets and their magnetic fields with RadioAstron. I. Imaging BL Lacertae at 21 Microarcsecond Resolution. *ApJ* 817, 96.  
 Greisen, E.W., 2003. AIPS, the VLA, and the VLBA. *Information Handling in Astronomy - Historical Vistas*. In: Heck, André (Ed.), *Astrophysics and Space Science Library*, vol. 285. Kluwer Academic Publishers, Dordrecht, pp. 109–125.  
 Johnson, M.D., Kovalev, Y.Y., Gwinn, C.R., et al., 2016. Extreme brightness temperatures and refractive substructure in 3c273 with RadioAstron. *ApJL* 820, L10.  
 Kardashev, N.S., Khartov, V.V., Abramov, V.V., et al., 2013. RadioAstron-A telescope with a size of 300,000 km: main parameters and first observational results. *Astron. Rep.* 57, 153–194.  
 Kardashev, N.S., Novikov, I.D., Lukash, V.N., et al., 2014. Review of scientific topics for the Millimetron space observatory. *Phys. Uspekhi* 57, 1199–1228.  
 Kardashev, N.S., Alakoz, A.V., Andrianov, A.S., et al., 2017. RadioAstron science program five years after launch: main science results. *Sol. Syst. Res.* 51, 535–554.  
 Kogan, L., 1996. Global ground VLBI network as a tied array for space VLBI. *VLBA Scient. Memo* 13, NRAO.  
 Komissarov, S.S., Falle, S.A.E.G., 1998. The large-scale structure of FR-II radio sources. *MNRAS* 297, 1087–1108.  
 Kovalev, Y.Y., Kardashev, N.S., Kellermann, K.I., et al., 2016. RadioAstron observations of the Quasar 3C273: a challenge to the brightness temperature limit. *ApJL* 820, L9.  
 Lobanov, A.P., Zensus, J.A., 2001. A cosmic double helix in the archetypical Quasar 3C273. *Science* 294, 128–131.  
 Lobanov, A.P., Gómez, J.L., Bruni, G., et al., 2015. RadioAstron space VLBI imaging of polarized radio emission in the high-redshift quasar 0642+449 at 1.6 GHz. *A&A* 583, A100.  
 Martí-Vidal, I., Marcaide, J.M., 2008. Spurious source generation in mapping from noisy phase-self-calibrated data. *A&A* 480, 289–295.  
 Matthews, L.D., Crew, G.B., Doeleman, S.S., et al., 2018. The ALMA phasing system: a beamforming capability for ultra-high-resolution science at (sub)millimeter wavelengths. *PASP* 130, 015002.  
 Müskens, A., Alef, W., Bertarini, A., et al., 2016. New DiFX Software Correlator Cluster at Bonn and Summary of Recent Activities. In: *International VLBI Service for Geodesy and Astrometry 2016 General Meeting Proceedings: New Horizons with VGOS*, pp. 171–175.  
 Nagai, H., Fujita, Y., Nakamura, M., et al., 2017. Enhanced polarized emission from the one-parsec-scale hotspot of 3C 84 as a result of the interaction with the clumpy ambient medium. *ApJ* 849, 52.  
 Nakamura, M., Asada, K., Hada, K., et al., 2018. Parabolic jets from the spinning black hole in M87. *ApJ* 868, 146.  
 Petrov, L., Kovalev, Y.Y., Fomalont, E.B., Gordon, D., 2011. The very long baseline array galactic plane survey-VGaPS. *AJ* 142, 35.

- Shepherd, M.C. 1997. Difmap: an Interactive Program for Synthesis Imaging. *Astronomical Data Analysis Software and Systems VI*. In: Hunt, Gareth, Payne, H.E. (Eds.), A.S.P. Conference Series, Astronomical Society of the Pacific, San Francisco, vol. 125, pp. 77–84.
- Tchekhovskoy, A., Narayan, R., McKinney, J.C., 2011. Efficient generation of jets from magnetically arrested accretion on a rapidly spinning black hole. *MNRAS* 418, L79–L83.
- Zamaninasab, M., Savolainen, T., Clausen-Brown, E., et al., 2013. Evidence for a large-scale helical magnetic field in the quasar 3C 454.3. *MNRAS* 436, 3341–3356.
- Zamaninasab, M., Clausen-Brown, E., Savolainen, T., et al., 2014. Dynamically important magnetic fields near accreting supermassive black holes. *Nature* 510, 126–128.